Liquefaction Ejecta Case Histories for 2010-11 Canterbury Earthquakes

Zorana Mijic, *Ph.D. Candidate, Depart. of Civil and Environmental Eng., Univ. of California, Berkeley, 441 Davis Hall, Univ. of California, Berkeley, CA 94720-1710, USA; email: zorana.mijic@berkeley.edu*
Jonathan D. Bray, *Professor, Depart. of Civil and Environmental Eng., Univ. of California, Berkeley, 453 Davis Hall, Univ. of California, Berkeley, CA 94720-1710, USA; email: jonbray@berkeley.edu*
Sjoerd van Ballegooy, *Expertise Director, Tonkin and Taylor, Ltd., 105 Carlton Gore Road, Newmarket, Auckland 1023, New Zealand; email: svanballegooy@tonkintaylor.co.nz*

ABSTRACT: *Liquefaction ejecta damaged the land and light-weight residential houses during the 2010-2011 Canterbury earthquakes. A database of well-documented field case histories that can be used to develop a procedure to estimate the settlement due to ejecta does not currently exist. In this paper, 235 case histories that document the occurrence and quantity of ejecta and its effects on infrastructure at 61 sites for each of the four primary earthquakes of the Canterbury sequence are presented. The case histories were developed with access to the geotechnical database that includes thousands of CPTs and boreholes, airborne LiDAR surveys, aerial photographs, and detailed property inspection reports in Christchurch, New Zealand. Direct measurements of ejecta were not available; hence, the ejecta-induced settlement values were estimated using LiDAR- and photographic-based approaches. The information related to ground conditions and seismic demand leading to differing quantities of ejecta-induced settlement during the Canterbury earthquake sequence were also described. This database of detailed ejecta case histories can be used to investigate the occurrence and effects of ejecta and to develop procedures to estimate the quantity of ejecta produced due to liquefaction.*

KEYWORDS: liquefaction, ejecta, case histories, Christchurch, earthquakes, photographs, LiDAR

SITE LOCATION: Geo-Database

INTRODUCTION

This paper summarizes the development of detailed liquefaction ejecta case histories for the four main events of the 2010-2011 Canterbury earthquake sequence (CES): the 4 Sep 2010 M_w 7.1, 22 Feb 2011 M_w 6.2, 13 Jun 2011 M_w 6.2, and 23 Dec 2011 M_w 6.1 events (see Figure 1). The 13 Jun 2011 earthquake was modeled as a M_w 6.2 earthquake to account for the excess pore water pressure that resulted from the first M_w 5.3 earthquake, and did not dissipate fully at the time of the second M_w 6.0 earthquake that occurred 80 min later (van Ballegooy et al., 2014). Based on piezometer measurements reported in T+T (2013), 25% of the excess pore water pressure generated by the first event was estimated to be present when the second earthquake occurred, which increased its effective magnitude by 0.2 based on magnitude-dependent liquefaction triggering curves. By the same reasoning, the Dec 2011 earthquake was modeled as a M_w 6.1 earthquake.

The extensive, repeated occurrence of liquefaction ejecta in the greater Christchurch area is virtually unprecedented in a modern urban setting. Liquefaction ejecta were a key mechanism of liquefaction-induced land damage and light-weight residential house damage during the CES (Rogers et al., 2015). Liquefaction affected 51,000 of 140,000 residential properties, damaging approximately 15,000 properties beyond economic repair. The level of infrastructure damage and the occurrence of liquefaction ejecta were strongly correlated. Areas without liquefaction ejecta or lateral spreading, although some likely had liquefaction at depth, typically had negligible liquefaction-induced land or building damage. Conversely, areas with liquefaction ejecta or lateral spreading had moderate-to-severe land or building damage (Rogers et al., 2015).

Submitted: 1 January 2022; Published: 29 August 2022
Reference: Mijic, Z., Bray, J. D., and van Ballegooy, S. (2022). Liquefaction Ejecta Case Histories for 2010-11 Canterbury Earthquakes. International Journal of Geoengineering Case Histories, Volume 6, Issue 3, pp. 73-93, doi: 10.4417/IJGCH-06-03-04

No procedures for estimating the occurrence and the amount of ejecta-induced settlement are currently available. There is no database with detailed case histories that could be used to develop the procedure or gain insights into the complex mechanism of ejecta, ground conditions, and seismic demand leading to the occurrence or non-occurrence of ejecta and the differing degrees of ejecta-induced settlement. The 2010-2011 CES represents an unprecedented opportunity for developing a liquefaction ejecta database that can be used as a basis for the development of procedures to evaluate the occurrence and amount of ejecta.

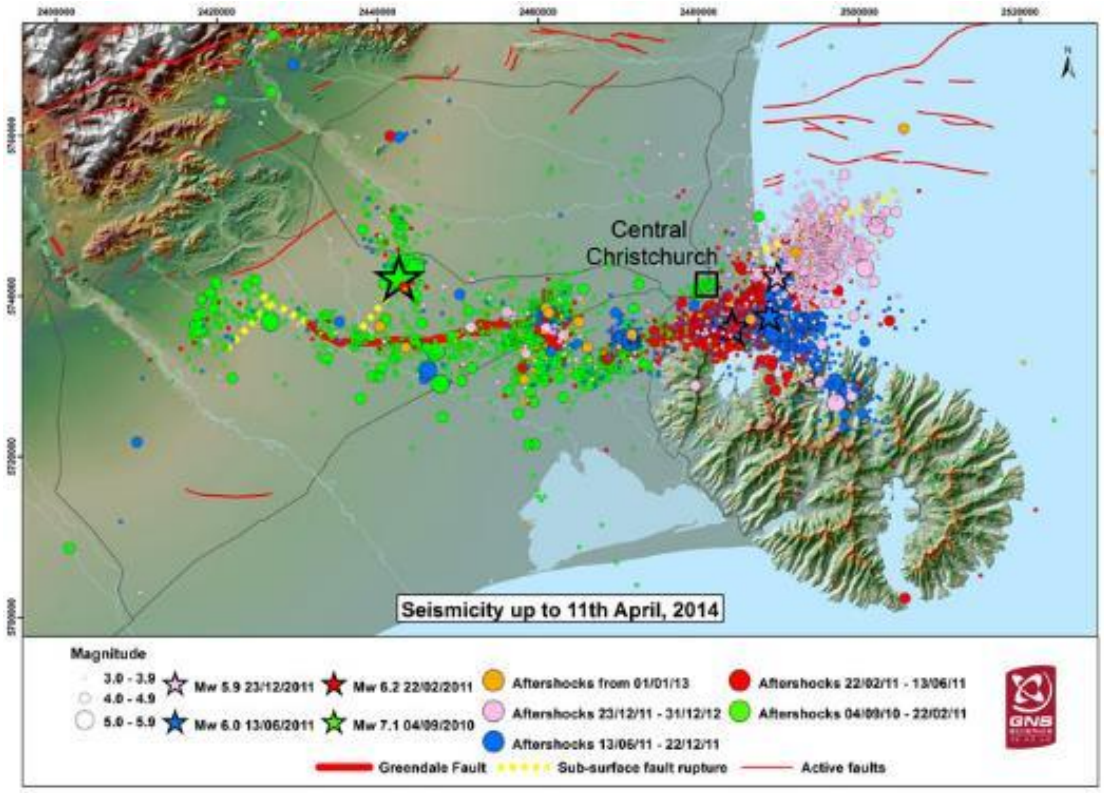


Figure 1. Location of 4 Sep 2010 Darfield main shock and subsequent aftershocks up to 11 Apr 2014 (GNS Science, 2021).

Liquefaction-induced ground deformation has three primary components: (1) shear-induced ground deformation resulting from soil-structure-interaction ratcheting and punching failure, (2) volumetric-induced deformation due to sedimentation and post-liquefaction reconsolidation, and (3) ejecta-induced ground deformation due to the loss of soil ejected onto the ground surface (Bray and Dashti, 2014). The shear-induced building settlement can be estimated using several methods (e.g., Bray and Macedo, 2017). The volumetric-induced settlement can also be estimated using several methods (e.g., Zhang et al., 2002). However, there is not a procedure for estimating the ejecta-induced ground settlement. The Liquefaction Severity Number, LSN, (van Ballegooy et al., 2014) and Liquefaction Potential Index, LPI, (Iwasaki et al. 1978) indices were not specifically developed to estimate the amount of liquefaction ejecta. Rough estimates of liquefaction ejecta occurrence and amounts can be made by the liquefaction ejecta demand, L_D, and crust resistance, C_R, parameters, a new procedure by Hutabarat and Bray (2022), but it requires additional validation with case history data.

Liquefaction ejecta tend to form in the presence of a low-permeability crust above the liquefied soil (Obermeier, 1996). A mixture of water and sediments is typically ejected onto the ground surface through preexisting gaps in the crust or dikes produced by hydraulic fracturing of the crust. In addition to ground motion characteristics (amplitude, frequency content, and duration), the severity of liquefaction manifestation at the ground surface is also influenced by the thickness and properties of the cap, characteristics of the underlying liquefying soil strata, and depositional environment (e.g., Beyzaei et al., 2018). A non-liquefying crust that is thicker than underlying liquefying soil strata tends to reduce the effects of liquefaction at the ground surface (van Ballegooy et al., 2014). Formation of ejecta is also affected by the built environment due to the load applied by infrastructure, disruption of an upward drainage path by an impervious constructed layer which may force the liquefied material to migrate sideways around it, and defects created in the crust, such as from light poles.

This paper summarizes the data that were used to conduct the research and explains the methodology used to estimate the ejecta-induced settlement to develop detailed ejecta case histories. The methodology is described for one illustrative site in Christchurch. Closing remarks regarding the research outcomes as well as guidance for future work are also provided.

DATA AND MATERIALS AVAILABLE

The scale and extent of land damage caused by the Canterbury earthquakes and having land insured for natural disaster damage in New Zealand (NZ) under the 1993 Earthquake Commission (EQC) Act resulted in a comprehensive geotechnical land damage assessment across Christchurch. The initial assessment of the extent and severity of the land damage through regional-scale mapping and rapid property-by-property mapping identified the areas that needed detailed EQC Land Damage Assessment Team (LDAT) inspection of individual properties (T+T, 2013). Following the detailed inspection of liquefaction-induced land damage at approximately 65,000 properties by assessment teams, over 25,000 cone penetration tests (CPTs), over 5,000 boreholes, many with piezometers installed, and several kilometers of geophysical surveys were conducted in Christchurch.

Sites throughout Christchurch were shaken multiple times and experienced no-to-extreme quantities of liquefaction ejecta (see Figure 2). The degree of liquefaction ejecta-induced damage varied from site to site and from earthquake to earthquake. Although direct measurements of ejecta after the Canterbury earthquakes are not available, liquefaction ejecta coverage and amounts for each of the four major Canterbury earthquakes can be characterized with access to the comprehensive T+T (2015) and LDAT (2021) databases. The T+T (2015) database contains aerial photographs for each earthquake, pre- and post-earthquake airborne Light Detection And Ranging (LiDAR) surveys, thousands of CPTs and boreholes with installed piezometers, earthquake-specific groundwater depth models, and robust estimates of PGA with uncertainties. The LDAT (2021) database is comprised of ground photographs and detailed land damage inspection notes.

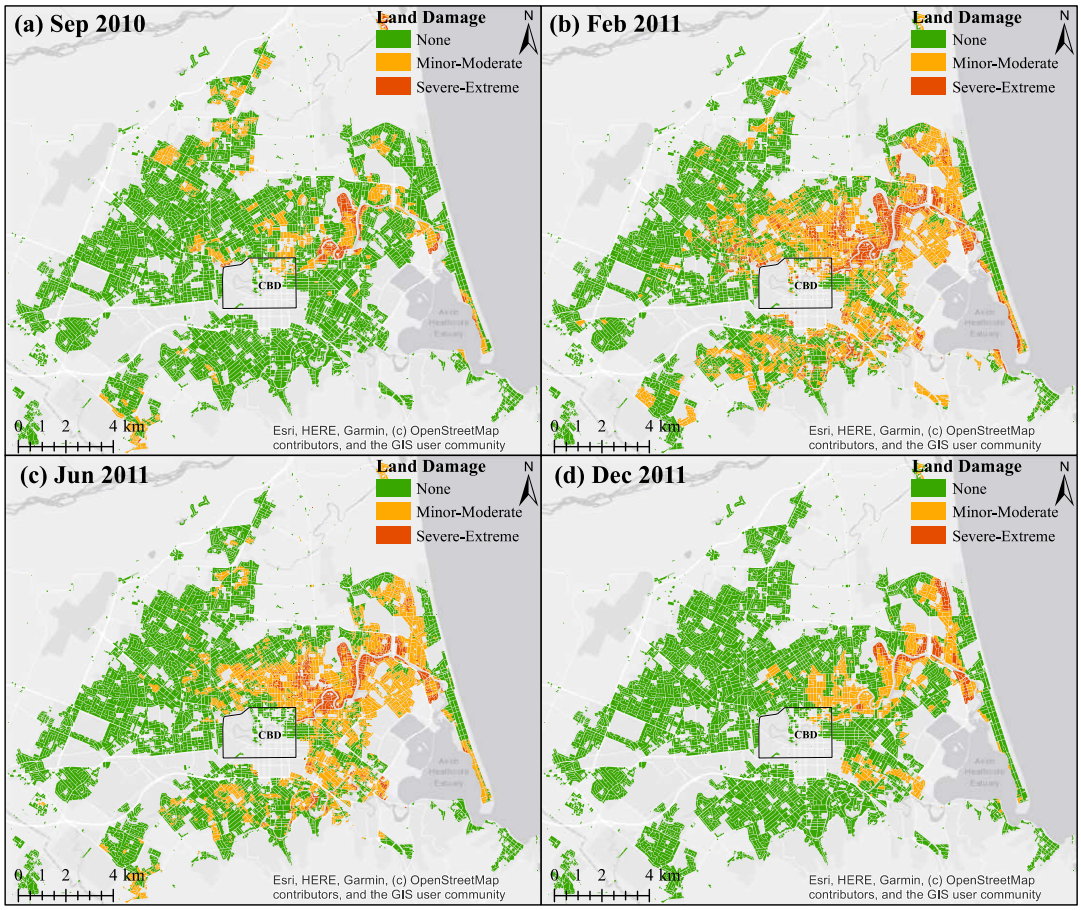


Figure 2. Liquefaction observations at the ground surface for the (a) 4 Sep 2010, (b) 22 Feb 2011, (c) 13 Jun 2011, and (d) 23 Dec 2011 earthquakes (T+T, 2015). (CBD = Christchurch Business District)

Airborne LiDAR Surveys

Airborne LiDAR surveys of Christchurch were conducted before and after each of the four main CES events to estimate the ground surface subsidence caused by each earthquake. The surveys were acquired by AAM Brisbane Pty. Ltd. and New Zealand Aerial Mapping (NZAM) Ltd. on (1) 6-9 Jul 2003, (2) 5 Sep 2010, (3) 8-10 Mar 2011, (4) 20-30 May 2011, (5) 18 and 20 Jul, 11 Aug, 25-27 Aug, and 2-3 Sep 2011, (6) 17-18 Feb 2012 (Russell and van Ballegooy, 2015), and (7) 25 Oct 2015. Thus, each LiDAR survey, apart from the Sep 2010 LiDAR survey, was flown at least a month after each main earthquake when much of the liquefaction ejecta were removed from most properties and roads. The position data points were acquired as a LiDAR survey point cloud and were classified as ground points or points that reflected off vegetation and structures (non-ground points). The accuracy of the acquired LiDAR points was verified against elevations of the Land Information New Zealand (LINZ) benchmarks that were surveyed before and after the main Canterbury earthquakes using GPS-based equipment and precise levelling (Russell and van Ballegooy, 2015; CERA, 2014). "The [vertical] accuracy of the LiDAR points relative to the LINZ benchmarks were estimated by subtracting the mean elevations of the LiDAR points around each LINZ benchmark from the surveyed elevation of the LINZ benchmark," which is referred to as the approximate error due to a typical vertical accuracy of ±30 mm of LINZ benchmark elevations (Russell and van Ballegooy, 2015). Low mean and median approximate errors suggest reasonable overall accuracy. Approximately 80% of the LiDAR point elevations for all post-Sep 2010 LiDAR surveys have a vertical accuracy of ±70 mm, while approximately 80% of the LiDAR point elevations for the Jul 2003 LiDAR survey are within ±150 mm of the LINZ benchmark elevations. The standard deviation of the approximate error for the Jul 2003 LiDAR survey is larger than for the post-Sep 2010 LiDAR surveys likely due to the lower density of LiDAR points and the lower precision in the LiDAR equipment in 2003 (Russell and van Ballegooy, 2015).

The ground classified points were also used to develop the bare earth digital elevation models (DEMs) that consist typically of 5 m by 5 m cells (Russell and van Ballegooy, 2015). Each cell represents an average ground surface elevation obtained by averaging the ground classified points within the DEM cell (Russell and van Ballegooy, 2015). The difference between a pre-earthquake DEM and a post-earthquake DEM can be used to estimate the change in vertical ground surface elevation due to an earthquake. However, there are limitations to estimating the ground surface subsidence from a difference DEM. The limitations include a localized error due to the interpolation of adjacent DEM cell elevations in areas with vegetation and buildings (thus fewer ground classified points) and the difference between the actual ground surface elevation and the average DEM elevation in areas with step changes in the ground surface (Russell and van Ballegooy, 2015). The difference DEMs can also be used to identify areas of greater uplift or subsidence due to anthropogenic changes (e.g., construction and vegetation removal) and error bands of apparent greater subsidence that are centered on and are parallel to individual LiDAR flight paths. These error bands are the artifacts of the LiDAR point acquisition as well as the post-acquisition processing that involves a combination of automated and manual classification of non-ground classified points. Detailed explanation of the accuracy and limitations of the DEMs and the LiDAR points is provided in Russell and van Ballegooy (2015).

Aerial Photography

High-resolution aerial photographs of Christchurch and its suburbs were acquired by NZAM after each main CES event – 5 Sep 2010, 24 Feb 2011, 14-15 Jun 2011, 16 Jun 2011, and 24 Dec 2011 – to identify areas with liquefaction ejecta to which inspection teams were dispatched to map damage. They were supplied as orthorectified, color-balanced, geolocated, tiled images and were transformed into image pyramids for efficient use (CGD, 2012a). The image locations may have some inaccuracy because the locations of the reference datums used during acquisition were not verified at the time of supply, in addition to an approximate, average 1 m residual error that stems from the orthorectification process (CGD, 2012a).

Detailed LDAT Property Inspection Mapping

About 65,000 properties in Christchurch and its suburbs were visually inspected in detail for liquefaction-related land damage to resolve the EQC land damage insurance claims (T+T, 2013). The inspection of individual properties was performed by the EQC LDAT, comprised of approximately 400 geotechnical engineers and engineering geologists (T+T, 2013). The LDAT used a land damage template to collect land damage information: lateral spreading, cracks, undulating land, local ponding, localized settlement causing drainage issues, new groundwater springs, and inundation of land with ejected soil. They also identified damage to any sloping land, retaining wall, foundation, and dwelling. Additionally, the LDAT used a property map with a recent aerial photograph to sketch locations of observed damage for each individual property. Liquefaction ejecta were often removed or eroded at the time of inspection, which makes the high-resolution aerial photographs an important supplement in assessing the extent of ejecta. The LDAT took photographs of ejecta remnants, sketched their approximate

locations on individual property maps, and often reported the maximum height of ejecta remnants. Claimants sometimes provided useful information regarding ejecta and its volume and height.

Conditional PGA

Robust estimates of conditional peak ground accelerations (PGAs) were developed for each main Canterbury earthquake as a combination of an empirical ground motion model and recordings at 19 strong motion stations within the Canterbury region (Bradley and Hughes, 2012a,b). The estimated PGAs were conditioned on the recorded PGAs at the strong motion stations to improve the fit of the generalized ground motion model for each earthquake. The conditional PGA at each location was estimated in terms of its median value and uncertainty (lognormal standard deviation). The accuracy of the estimated PGA increases with the increasing proximity to the strong motion stations. For site locations that are far from the strong motion stations, the conditional distribution of PGA is similar to the unconditional distribution of PGA. For sites close to the strong motion stations, the conditional distribution approaches the PGA value recorded at the station (Bradley and Hughes, 2012a). The PGAs are available in the form of contour maps (CGD, 2015).

Event-Specific Groundwater Depths

The event-specific groundwater depths are based on water level measurements from wells installed prior to and after the 4 Sep 2010 earthquake and the most appropriate LiDAR-derived DEM (CGD, 2014). Groundwater levels in the wells were converted to free surface elevations based on surveyed well-head levels. The elevations at the wells and the adjacent rivers prior to each main Canterbury earthquake were used to develop surface models that were subtracted from the corresponding LiDAR DEM. The obtained groundwater depths are based on the mean free surface elevations at the time of each earthquake. In case of geographical sparsity of wells for earlier earthquakes, water level measurements at the newly installed wells were used to extrapolate the free surface elevations back in time. The fitted surface models for each earthquake are color-banded and available as an image pyramid (CGD, 2014).

SITES USED FOR THE DEVELOPMENT OF CASE HISTORIES

The NZ-US researchers developed a comprehensive dataset of 55 Christchurch sites to investigate liquefaction triggering aspects in detail. The dataset includes field investigation data (e.g., CPT measurements and sonic borehole logs), liquefaction observations using aerial photographs, coarse estimates of liquefaction-related ground surface subsidence based on the LiDAR-derived difference DEMs, liquefaction-induced damage indices, etc. However, as is the case for all of Christchurch, direct measurements of liquefaction ejecta were not conducted at these sites. The dataset consists predominantly of sites that had the severity of surficial manifestation of liquefaction misestimated by simplified liquefaction triggering methods and liquefaction-induced damage indices. The “55 sites” data are discussed in Russell and van Ballegooy (2015) and are used in several research papers (e.g., Cubrinovski et al., 2017). In this study, 27 sites from the “55 sites” dataset were investigated in detail and an additional 8 sites had coarse analyses performed because they had no-to-minor ejecta, no LiDAR surveys, or only one CPT. The remaining 20 sites of the “55 sites” were not used due to lateral spreading, topographical features, and ejecta that were not recognizable in the aerial photographs but whose occurrence was suggested by the property inspection reports.

An additional 34 sites, primarily from the NE quadrant of Christchurch, were selected to form a database with no-to-extreme liquefaction ejecta case histories. The NE quadrant had the most predominant liquefaction ejecta-induced damage and was without significant discrepancies between observations and estimations of liquefaction-induced damage according to the preliminary regional-scale assessment of the LSN and LPI accuracy in the site selection process (e.g., using the LPI accuracy map for Christchurch developed by Maurer et al., 2014). Additionally, these were high-quality sites with good observations (i.e., aerial and ground photographs and EQC LDAT property inspection reports), reliable settlement estimates based on the LiDAR survey data, at least two closely spaced CPTs with investigation depths of 15-20 m, and a nearby borehole. These 34 sites and the 27 detailed sites from the “55 sites” dataset were used to build 235 detailed case histories (i.e., 58 sites times four earthquakes plus 3 sites times one earthquake due to lateral spreading in the other events). Figure 3 illustrates the site locations. All details related to the case histories are provided as an electronic supplement as Appendix A.1 through Appendix A.61 (hereinafter referred to as Appendix A). The important information related to each site and each earthquake is provided in the *EjectaCaseHistories_FlatFile.xlsx* spreadsheet as an electronic supplement to this paper.

METHODOLOGY

Each site was centered on a CPT or cross-hole shear wave velocity (V_s) survey location, and encompassed an area within a 50-m radius of its center (termed a 50-m buffer) due to the spatial variation in ejecta distribution and presence of buildings. However, the 10-m and 20-m radii (10-m and 20-m buffers, respectively) were used primarily in the analyses. A site was first inspected for the presence of free-face features, sloping land, retaining walls, buildings, vegetation, pavement, and anthropogenic changes, as they could affect liquefaction manifestation at the ground surface and LiDAR survey measurements. This information for each site can be found in each site description in Appendix A. Supporting figures for each site are also included in Appendix A. An area free of vegetation, buildings, anthropogenic changes, and with representative distribution of ejecta for the site was selected for detailed settlement assessment. Other important information, including the soil profile category, PGA, groundwater depth, crust thickness, LPI, LSN, L_D, C_R, ejecta pattern, ejecta distribution, and ejecta quantum for each case history are provided in the *EjectaCaseHistories_FlatFile.xlsx* spreadsheet. The discrepancy between the liquefaction severity indices and the ejecta coverage is also provided.

As mentioned previously, direct measurements of ejecta amounts were not made. Two alternative methods for estimating the free-field ejecta-induced settlement were employed. The photographic-based method involved the use of aerial and ground photographs, EQC LDAT property inspection reports and maps, and geometrical approximations of the ejected soil shapes. The second method was based on LiDAR point elevations and one-dimensional, free-field volumetric-induced settlement for level ground as per Zhang et al. (2002). The best final estimate of the ejecta-induced settlement was determined as the weighted average of the two estimates.

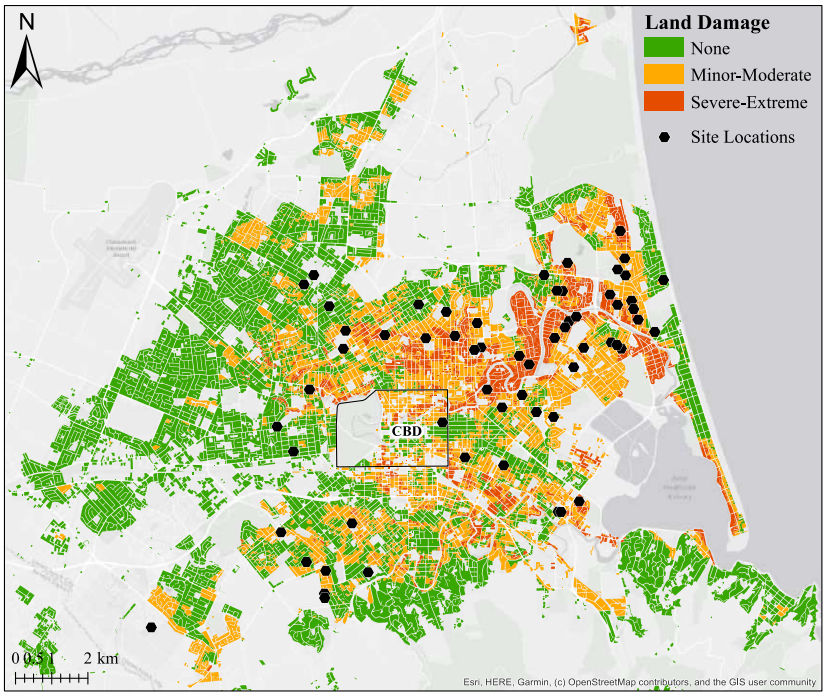


Figure 3. The maximum liquefaction ejecta-induced damage map (T+T, 2015) with site locations. (CBD = Christchurch Business District)

Photographic-Based Ejecta-Induced Settlement

To obtain the photographic-based settlement due to ejecta, $S_{E,P}$, the shape of ejecta manifestations was estimated. Ejecta were typically shaped as a prism with irregular curvilinear bases, prism with triangular bases, isolated and naturally occurring cone, and artificially formed pile as a result of cleaning. The portion of the assessment area covered by ejecta was quantified using Google Earth Pro by outlining the coverage area on the high-resolution aerial photograph for each earthquake. The available photographs, reports, and geometrical approximations were used to estimate the height of ejecta.

For ejecta shaped as a prism with irregular curvilinear bases (see Figure 4a), the differing thicknesses of ejecta were identified on a high-resolution aerial photograph as having different colors (i.e., darker colors were assumed to correspond to thicker ejecta layers because of the longer time required to dry the soil) and the corresponding areas were measured using a polygon tool in Google Earth Pro. The height of each ejecta layer was estimated based on the available ground photographs, LDAT property inspection maps, reports that occasionally included the height of ejecta remnants, visibility of the ejecta layer in the aerial photograph, and measurements of the ejecta height in neighboring, similarly affected areas. The volume of ejecta shaped as a prism with irregular curvilinear bases, $V_{E,thick+thin}$, was then estimated as

$$V_{E,thick+thin} = \sum_{i=1}^{m} A_{E,thick,i} * H_{E,thick,i} + \sum_{j=1}^{n} A_{E,thin,j} * H_{E,thin,j} \quad (1)$$

where $A_{E,thick,i}$ and $H_{E,thick,i}$ are the area and the height, respectively, of an i^{th} thick ejecta layer, while $A_{E,thin,j}$ and $H_{E,thin,j}$ are the area and the height, respectively, of a j^{th} thin ejecta layer.

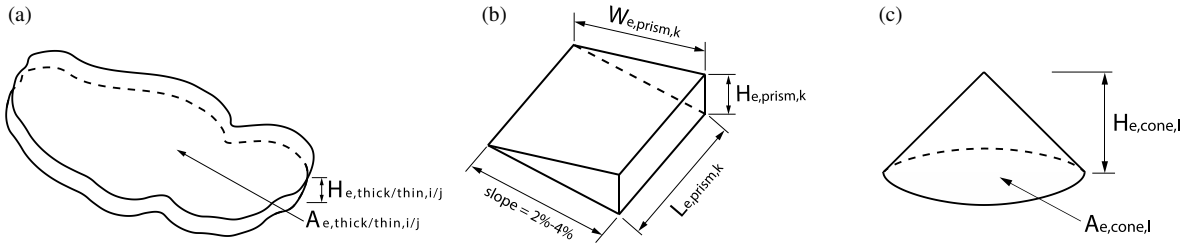


Figure 4. (a) Ejecta shaped as a prism with irregular curvilinear bases, (b) ejecta on the road shaped as a prism with triangular bases, and (c) ejecta occurring naturally as a cone.

Ejecta on the road were typically shaped as a series of triangular-base prisms with different dimensions (see Figure 4b). The rectangular shapes of ejecta on the road were outlined on the high-resolution aerial photograph for each earthquake, and their dimensions were measured using the Google Earth Pro tools. The width of a rectangle, $W_{E,prism,k}$, is perpendicular to the curb, while the length of a rectangle, $L_{E,prism,k}$, aligns with the curb. The lower and upper estimates of the height of ejecta at the curb, $H_{E,prism,k}$, were based on the typical cross-slopes of normal crown of 2% and 4%, respectively. The height of ejecta was capped at a typical curb height of 150 mm unless ejecta extended above the curb and onto the ground surface toward properties. The volume of ejecta shaped as a triangular-base prism, $V_{E,prism}$, was estimated as

$$V_{E,prism} = \frac{1}{2}\sum_{k=1}^{p} W_{E,prism,k} * H_{E,prism,k} * L_{E,prism,k}. \quad (2)$$

Ejecta that occurred naturally in a form of an isolated cone (see Figure 4c) had its area $A_{E,cone,l}$ measured on a high-resolution aerial photograph in Google Earth Pro, and its height $H_{E,cone,l}$ estimated based on the best available physical evidence to obtain the volume, $V_{E,cone}$, as

$$V_{E,cone} = \frac{1}{3}\sum_{l=1}^{r} A_{E,cone,l} * H_{E,cone,l}. \quad (3)$$

When ejecta were cleaned from properties and roads into a pile, the pile consisted usually of an isolated cone or partially overlapping cones of ejecta with an assumed angle of repose of 30° (similar in shape to Figure 4c). The radius and the area of a cone's circular base, $R_{E,cc,s}$ and $A_{E,cc,s}$, respectively, were measured in Google Earth Pro, and the height of a conically shaped pile component, $H_{E,cc,s}$, was approximated as $R_{E,cc,s} * \tan(30°)$. The volume of piled ejecta was estimated using Eq. 3.

The volumes of all differently shaped ejecta present within a settlement assessment area were summed and divided by the total settlement assessment area, A_T, to obtain the areal ejecta-induced settlement, S_{E,P_areal} (also denoted as $S_{E,P}$). In addition, the photographic-based localized ejecta-induced settlement, $S_{E,P_localized}$, was calculated as the total volume of ejecta, V_E, divided by only the area covered by ejecta, A_E. If ejecta did not completely cover A_T, S_{E,P_areal} was lower than $S_{E,P_localized}$ due to its areal averaging of ejecta-induced settlement. The S_{E,P_areal} and $S_{E,P_localized}$ values for each case history and all supporting estimates are provided in Appendix A.

LiDAR-Based Ejecta-Induced Settlement

The first step in estimating the free-field ejecta-induced settlement using the LiDAR-based approach was to identify the location of a site relative to the LiDAR flight error bands and the zones of overestimated (and underestimated) ground surface subsidence (CGD, 2012b) to account for errors, and to estimate the vertical tectonic movement of a site for each earthquake (CGD, 2012b). The adjustments for each earthquake event at each site due to the global offset, i.e., due to subtracting the post-earthquake ground surface elevations from the pre-earthquake ground surface elevations wherein both the pre-earthquake and post-earthquake LiDAR survey point elevations have an approximate median error (the accuracy of the measured elevations relative to the corresponding LINZ benchmarks), are summarized in Appendix A.

LAS files containing LiDAR point cloud data were imported into Global Mapper to estimate the ground surface elevation within each site's settlement assessment area. After removing visible vegetation, buildings, and similar features, the remaining points were selected to compute the average ground surface elevation (a centroid of the selected points). This was performed for each LiDAR survey to evaluate the change in the ground surface elevation due to each earthquake. For instance, the change in the ground surface elevation within the settlement assessment area due to the 4 Sep 2010 earthquake was calculated by subtracting the average ground surface elevation of the 5 Sep 2010 LiDAR survey points from the average ground surface elevation of the Jul 2003 LiDAR survey points. The earthquake-induced change in ground surface elevation is provided for each site in the Appendix A (termed as raw liquefaction-related ground surface subsidence using original LiDAR points). These values were then adjusted for the LiDAR flight error, vertical tectonic movement, global offset, and presence of ejecta at a site at the time of a LiDAR survey. The obtained liquefaction-induced ground surface subsidence, S_T, for each earthquake is provided in Table 6 of each site description in Appendix A.

Considering that liquefaction effects in Christchurch were not significant for earthquakes other than the main four events, the LiDAR surveys repeated after the Feb 2011 and Dec 2011 earthquakes provided an estimate of the repeat measurement error as the absolute difference between the Mar 2011 and May 2011 ground surface elevations and the Feb 2012 and Oct 2015 ground surface elevations averaged over the assessment area. The standard deviations available for each set of pre-earthquake and post-earthquake LiDAR surveys were combined to account for the effect of areal averaging of the surveyed elevations on the standard deviation of the LiDAR measurement error for individual points (the accuracy of the supplied LiDAR points relative to the LINZ benchmarks) for each LiDAR survey provided by Russell and van Ballegooy (2015). The standard deviation obtained for each main Canterbury earthquake was then multiplied by the maximum percent change in standard deviation (i.e., the maximum ratio of the repeat measurement error and the standard deviation for individual points). The adjusted standard deviation values are provided in Table 4 of each site description in Appendix A.

As a rough check, the estimated liquefaction-induced ground surface subsidence for each earthquake was compared with the coarse estimate of liquefaction-induced ground surface subsidence based on the difference between the corresponding pre- and post-earthquake LiDAR DEMs (the difference DEM). The latter values had to be corrected for the appropriate LiDAR flight errors and the presence of ejecta at a site at the time of a LiDAR survey. The LiDAR DEM-based values of liquefaction-induced settlement were not used in calculations of the ejecta-induced settlement.

The volumetric settlement due to sedimentation and post-liquefaction reconsolidation, S_{V1D}, was subtracted from the total liquefaction-induced settlement, S_T, to obtain the free-field liquefaction ejecta-induced settlement, $S_{E,L}$ (see Table 8 of each site description in Appendix A). The shear-induced ground settlement was neglected because the selected case histories originated from the free-field sites. The S_{V1D} was computed in Cliq v.3.0.3.2 (Ioannides, 2019) with the CPTs presented in Appendix A using the Zhang et al. (2002) procedure, which used the factor of safety against liquefaction, FS_L, from the Boulanger and Idriss (2016) procedure. The input parameters were the median PGA by Bradley and Hughes (2012a,b), probability of liquefaction, P_L, of 50%, I_c cutoff value of 2.6 as a threshold between liquefiable and non-liquefiable soil (Lees et al., 2015), C_{FC} of 0.13 developed for Christchurch soil by Maurer et al. (2019), and the groundwater depth at the time of each earthquake (CGD, 2014). The average S_{V1D} for each settlement assessment area was estimated for each earthquake and is reported in Table 8 of each site description in Appendix A. The sensitivity of volumetric settlement to PGA, C_{FC}, and P_L for each earthquake event was derived for two sites (VsVp 57203 – Shirley Intermediate School and CPT 5586 – Vivian St). The arithmetic mean of the range of the minimum and maximum difference was evaluated for each assessment area of the two sites. The maximum arithmetic mean for each earthquake event was rounded to the nearest five millimeters and was used as the uncertainty value. Accordingly, the volumetric settlement uncertainties of ± 20, ± 50, ± 25, and ± 50 mm for the Sep 2010, Feb 2011, Jun 2011, and Dec 2011 earthquakes, respectively, were used for all sites in this study.

Best Estimate of Ejecta-Induced Settlement

The best estimate of the ejecta-induced settlement, $S_{E,final}$, was calculated as the weighted average of the two estimates per the photographic evidence-based method, $S_{E,P}$, and the LiDAR-based method, $S_{E,L}$ (see Table 11 of each site description in Appendix A). The weighting coefficients were based on the LiDAR measurement errors, misestimates of liquefaction severity using the liquefaction triggering procedures as per Maurer et al. (2014), and completeness of visual evidence. Table 1 summarizes the best estimates of the ejecta-induced free-field settlement for the 61 sites.

Table 1. Best estimates of areal ejecta-induced free-field settlement for each site.

Site Name	Site ID	Long. (deg)	Lat. (deg)	SPC	Ejecta-Induced Free-Field Settlement (mm)			
					Sep 2010	Feb 2011	Jun 2011	Dec 2011
Shirley Intermediate School	VsVp 57203	172.661995	-43.510408	1	0	125 ±25	50 ±15	<5
Rydal Reserve	VsVp 57190	172.608493	-43.565806	4	<5	30 ±10	0	0
Rawhiti Domain	VsVp 57188	172.721404	-43.506685	1	0	0	0	0
Caulfield Ave	VsVp 38175	172.548658	-43.579706	4	<5	0	0	0
70 Langdons Rd	VsVp 57142	172.604872	-43.492195	3	0	0	0	0
Vivian St	CPT 5586	172.689983	-43.496445	1	0	80 ±30	50 ±30	<5
50 Eureka St	VsVp 57195	172.706500	-43.509273	1	0	70 ±70	<5	0
Parnwell St & Bassett St	CPT 27709	172.687992	-43.496341	1	0	90 ±25	20 ±10	5 ±5
Vangelis Ln & Fernbrook Pl	CPT 49582	172.650158	-43.501489	1	0	10 ±5	0	<5
Pinewood Ave	CPT 61991	172.711272	-43.488333	1	0	25 ±5	10 ±5	5 ±5
Carisbrooke Playground	VsVp 57193	172.709944	-43.510815	1	0	<5	0	0
Avondale Playground	VsVp 57062	172.687194	-43.508109	1	0	60 ±45	35 ±65	0
Bower Ave	CPT 3937	172.711488	-43.492600	1	0	95 ±35	20 ±5	10 ±5
Wattle Dr	CPT 90678	172.706167	-43.497325	1	0	120 ±30	85 ±25	65 ±15
Warrington St	CPT 44959	172.643107	-43.508034	1	5 ±5	40 ±10	15 ±20	<5
Hunt Ln	CPT 4674	172.692150	-43.503948	1	0	90 ±30	20 ±20	5 ±5
Sandown Cres	CPT 15498	172.708479	-43.509917	1	0	50 ±10	10 ±5	0
Travis Country Dr	CPT 29778	172.691683	-43.489401	1	0	15 ±20	<5	<5
Aldershot St	CPT 5261	172.697064	-43.510579	1	0	130 ±35	50 ±15	25 ±5
1/19 Chardale St	VsVp 57320	172.694632	-43.502797	1	5 ±5	--	--	--

Site Name	Site ID	Long. (deg)	Lat. (deg)	SPC	Ejecta-Induced Free-Field Settlement (mm)			
					Sep 2010	Feb 2011	Jun 2011	Dec 2011
15b Royds Pl	VsVp 57326	172.603276	-43.520686	4	0	--	--	--
31 Landy St*	CPT 44439	172.678436	-43.514681	1	25 ±5	50 ±10	40 ±10	10 ±5
Normans Rd/Papanui Rd	VsVp 57200	172.615699	-43.506100	4	0	--	--	--
St. Teresa's School	VsVp 57191	172.592135	-43.529873	2	0	0	0	0
Kaiwara Reserve	VsVp 57182	172.608046	-43.571492	3	0	10 ±5	0	0
Ti Rakau Reserve	VsVp 57186	172.695373	-43.548825	1	0	100 ±15	85 ±10	5 ±5
Avondale Park	VsVp 57187	172.690763	-43.505496	2	0	20 ±10	10 ±5	5 ±5
Sabina Playground	VsVp 57192	172.660660	-43.504340	1	0	50 ±10	30 ±10	5 ±5
Barrington Park	VsVp 38172	172.617541	-43.554035	2	0	15 ±5	<5	0
Shortland St	CPT 6551	172.693665	-43.515402	1	0	25 ±25	25 ±20	0
Mark Treffers Dr	CPT 62594	172.708784	-43.491115	1	0	35 ±10	10 ±5	5 ±5
Shirley Primary School	CPT 54376	172.653071	-43.507478	1	0	75 ±25	25 ±5	0
Cashmere High School	CPT 33732	172.623013	-43.566259	1	0	65 ±20	0	0
Dunarnan St	CPT 24039	172.675985	-43.522271	1	0	40 ±25	20 ±20	10 ±5
Baker St	CPT 14070	172.715770	-43.503609	1	0	155 ±40	105 ±10	120 ±20
Randolph St	CPT 44440	172.669546	-43.539782	1	0	90 ±20	30 ±5	0
Woodham Rd	CPT 25514	172.669086	-43.525337	1	0	5 ±5	5 ±5	0
Rudds Rd	CPT 5687	172.686716	-43.527755	1	0	35 ±10	15 ±5	0
Palmers Rd	CPT 27040	172.713519	-43.498906	1	0	95 ±30	75 ±55	15 ±5
Willryan Ave	CPT 2168	172.708731	-43.499905	1	0	55 ±30	35 ±35	5 ±5
Bideford Pl	CPT 17200	172.675071	-43.512497	1	<5	90 ±30	25 ±20	0
Wharenui School	VsVp 57165	172.597625	-43.536096	2	0	0	0	0
Heaton Normal Intermediate School	VsVp 57181	172.614886	-43.510572	2	40 ±10	25 ±10	15 ±5	<5
Hillmorton High School	VsVp 57201	172.593252	-43.556187	3	0	10 ±5	0	0

Site Name	Site ID	Long. (deg)	Lat. (deg)	SPC	Ejecta-Induced Free-Field Settlement (mm)			
					Sep 2010	Feb 2011	Jun 2011	Dec 2011
St. Albans Catholic School	VsVp 57180	172.629117	-43.507198	2	0	5 ±5	<5	0
113A Palmers Rd	CPT 29740	172.714230	-43.500972	1	0	80 ±45	70 ±40	65 ±20
Hurst Pl	CPT 25981	172.709763	-43.481524	1	0	60 ±15	25 ±10	30 ±5
Shirley Boys High School	CPT 56468	172.659684	-43.511008	1	0	25 ±10	25 ±20	10 ±5
Bracken St	CPT 59661	172.663966	-43.520893	1	40 ±10	75 ±10	25 ±5	15 ±5
Palinurus Rd 1	VsVp 57185	172.688215	-43.551331	1	0	0	0	0
Palinurus Rd 2	CPT 62761	172.689145	-43.551414	1	0	35 ±10	30 ±5	0
Nursery Rd	CPT 17262	172.656360	-43.537748	2	0	60 ±15	10 ±5	0
Gainsborough Reserve	VsVp 38176	172.601913	-43.563623	3	0	0	0	0
455 Papanui Rd	VsVp 57189	172.610136	-43.499954	3	0	0	0	0
Keers Rd	CPT 28986	172.680817	-43.526519	1	0	0	0	0
200 Cashmere Rd	VsVp 38171	172.608100	-43.572615	2	0	0	0	0
Armagh St	CPT 45795	172.648678	-43.529008	1	0	0	0	0
Lakewood Dr	CPT 54736	172.683682	-43.492444	1	0	0	0	0
Kensington Ave	CPT 88252	172.640665	-43.499634	2	0	0	0	0
Tonks St	CPT 128494	172.724500	-43.493746	1	0	0	0	0
Marblewood Reserve	VsVp 57155	172.601543	-43.494509	3	0	0	0	0

Note: SPC = Soil Profile Categories, which can be defined as (1) thick, clean sand, (2) partially stratified, (3) highly stratified silty soil, and (4) gravel-dominated soil profile; * VsVp site moved to CPT.

DETAILED EVALUATION OF THE SHIRLEY INTERMEDIATE SCHOOL CASE HISTORIES

The detailed evaluation of one site is presented to illustrate the methods employed to develop the ejecta-induced ground settlement case histories. The Shirley Intermediate School site (see Table 1) is a level, open-field site covered largely in grass and did not undergo lateral spreading during the Canterbury earthquakes. The nearest free-face feature is a creek that is approximately 55 m from the center of the site. Ten percent of the site's 50-m buffer is occupied by school buildings, which were constructed between Apr 2011 and Jun 2011, and 15% of the site is covered by a road. Some minor earthwork was performed in the building area between Oct 2009 and Feb 2011. Trees, bushes, and plants other than grass (all termed vegetation) cover 10% of the 20-m buffer and 20% of the 50-m buffer. All these features and anthropogenic changes were considered when selecting the settlement assessment area, as they could affect the LiDAR survey measurements. The area selected for the ejecta-induced settlement analysis excludes vegetation, buildings, and significant anthropogenic changes (see Figure 5). This area also has good spatial distribution of ejecta (see Figure 6).

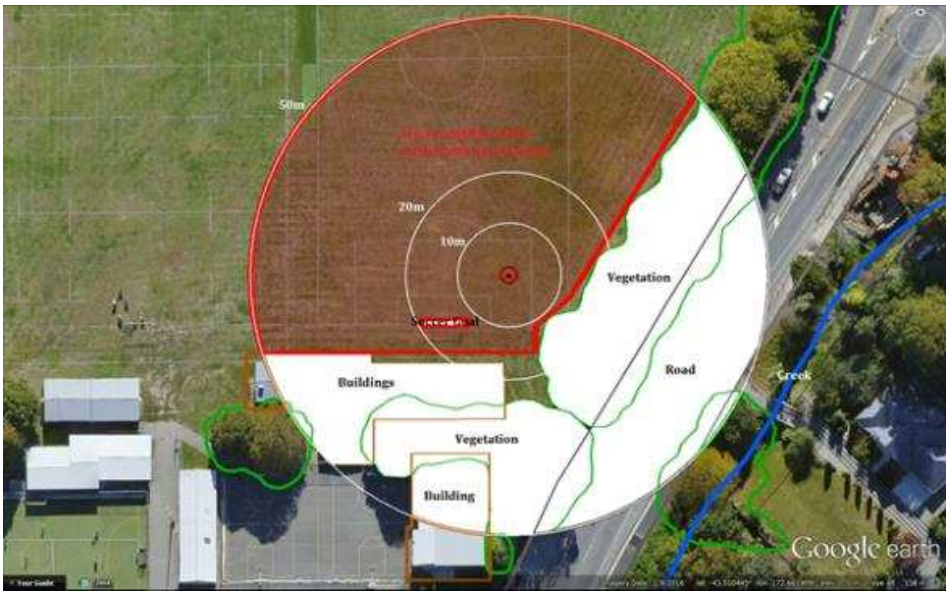


Figure 5. The Shirley Intermediate School site plan with the area analyzed for ejecta-induced settlement.

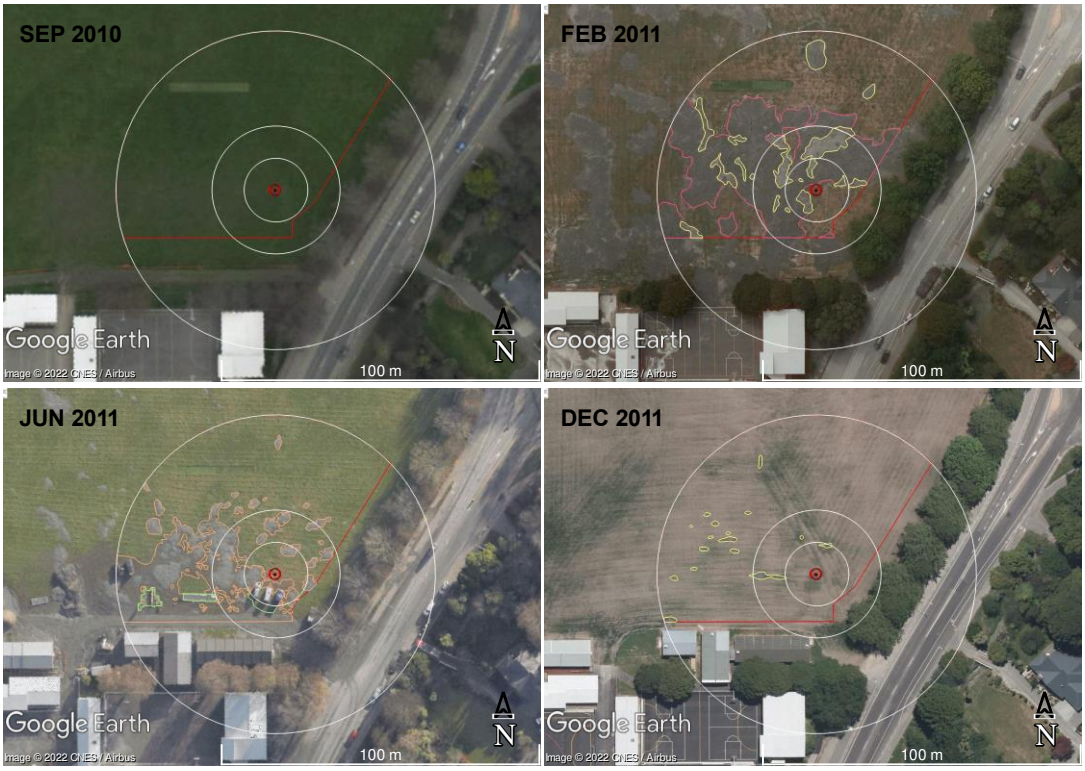


Figure 6. Aerial photographs acquired for Shirley Intermediate School in Sep 2010, Feb 2011, Jun 2011, and Dec 2011 (CGD, 2012a) with ejecta outlines for the 10-, 20-, and 50-m buffers.

The aerial photographs in Figure 6 were used to estimate the occurrence of ejecta and to measure the area of ejecta coverage within the assessment area (the red outline). The absence of ejecta is evident for the Sep 2010 earthquake. For the Feb 2011 earthquake, ejecta occurred across the site in a pattern of interconnected soil deposits originating from different fissures and forming irregularly shaped ejecta blankets rather than in a pattern of individual conically shaped soil boils. Different shades of gray of the ejecta were interpreted as different ejecta thicknesses. The light gray ejecta outlined in yellow were classified

as thin ejecta, while the dark gray ejecta outlined in pink were classified as thick ejecta. The total areas of the outlined thick ejecta layers and the outlined thin ejecta layers ($A_{E,thick}$ and $A_{E,thin}$, respectively) were measured in Google Earth Pro. The $A_{E,thick}$ and $A_{E,thin}$ values for the 10-m buffer are summarized in Table 2. In the absence of ground photographs, the height range for the thick and thin ejecta layers ($H_{E,thick}$ and $H_{E,thin}$, respectively) was estimated based on the typical height of similar-looking ejecta for the neighboring area and observations made by people (Table 2). Finally, the volume of ejecta was estimated using Eq. 1 and was divided by the total assessment area, A_T, to obtain the areal ejecta-induced free-field settlement, S_{E,P_areal} (Table 3), while the localized ejecta-induced settlement, $S_{E,P_localized}$ (Table 3) was obtained by dividing the total volume of ejecta within A_T by the coverage area of ejecta, A_E. Figure 6 also shows the presence of ejecta for the Jun 2011 earthquake. However, ejecta appeared to be partially cleaned from the site. To account for this uncertainty, the height of ejecta was provided as a wider range, while assuming ejecta covered the portion of the site in light brown color. The area for the Jun 2011 earthquake reported in Table 2 corresponds to the area outlined in orange and within the 10-m buffer. Also, cars, shadows, and construction equipment obscured a portion of the assessment area in the Jun 2011 aerial photograph, resulting in that portion of the site being excluded from the analysis. For the Dec 2011 earthquake, only minor ejecta (outlined in yellow in Figure 6) were present.

Table 2. Coverage area and height of ejecta estimates for 10-m buffer using photographs.

Earthquake Event	$A_{E,thick}$ (m^2)	$H_{E,thick}$ (mm)	$A_{E,thin}$ (m^2)	$H_{E,thin}$ (mm)	A_T (m^2)
Sep 2010	0	0	0	0	314
Feb 2011	143	150-250	39	50-100	314
Jun 2011	94	30-100	0	0	269*
Dec 2011	0	0	3	10-20	314

Notes: A_T = Total assessment area of a buffer being considered; * indicates that A_T is lower due to the presence of vehicles and their shadows at portions of the site when the aerial photograph was acquired.

Table 3. Photographic-based areal and localized ejecta-induced settlement.

Earthquake Event	10-m Buffer		20-m Buffer		50-m Buffer	
	S_{E,P_areal} (mm)	$S_{E,P_localized}$ (mm)	S_{E,P_areal} (mm)	$S_{E,P_localized}$ (mm)	S_{E,P_areal} (mm)	$S_{E,P_localized}$ (mm)
Sep 2010	0	0	0	0	0	0
Feb 2011	100±25	175±45	130±35	175±45	75±20	175±45
Jun 2011	25±10	65±35	30±15	65±35	20±10	65±35
Dec 2011	<5	15±5	<5	15±5	<5	15±5

Note: The estimates are rounded to the nearest 5 mm.

To estimate the LiDAR-based ejecta-induced settlement, the change in the ground surface elevation within the assessment area was determined for individual LiDAR points, such as those shown in Figure 7, for each earthquake (Table 4). These values were then adjusted for the LiDAR flight error, global offset, and tectonic movement (Table 5). The site is in the apparent zone of higher ground surface subsidence for the Sep 2010 earthquake and the apparent zone of lower ground surface subsidence for the Feb 2011 earthquake (Figure 8). To account for this LiDAR flight error, 100 mm were subtracted from the ground surface elevation change in Table 4 for the Sep 2010 earthquake and 100 mm were added to the ground surface elevation change in Table 4 for the Feb 2011 earthquake. The final estimates of liquefaction-induced ground surface subsidence provided in Table 6 were compared with the coarse estimates of the ground surface subsidence using the LiDAR DEMs (Figure 9). No major discrepancies between the two sets of estimates were observed. The average S_{V1D} was then calculated and subtracted from the values in Table 6 to obtain $S_{E,L}$ (Table 7). The PGA ranged from 0.19 g for the Sep 2010 earthquake to 0.38 g for the Feb 2011 earthquake. The depth to groundwater was in the range from 2.0 m below ground surface (BGS) for the Dec 2011 earthquake to 2.5 m BGS for the Sep 2010 and Feb 2011 earthquakes. All CPTs shown in Figure 10 were used to calculate the average S_{V1D} for the 50-m buffer (four of them were outside the 50-m buffer; CPT 55672 was 90 m away from the center of the site), whereas only CPTs 56473 and 57366 were used to calculate the average S_{V1D} for the 10-m and 20-m buffers. The S_{V1D} values for individual CPTs for each earthquake event are provided in Table 8. Figure 11 illustrates the cyclic resistance ratio (CRR) and the cyclic stress ratio (CSR) for each main earthquake event, which were computed in Cliq v.3.0.3.2 for CPTs 56473 and 57366 using the Boulanger and Idriss (2016) procedure.

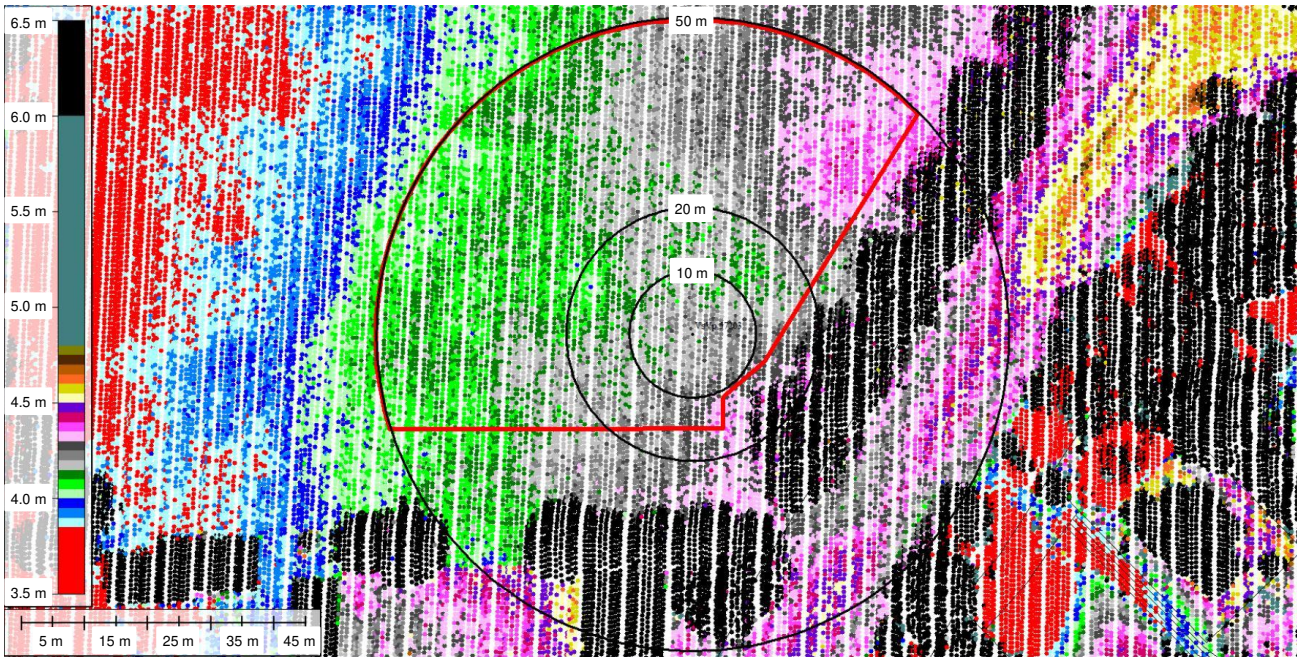


Figure 7. LiDAR survey points used to compute the average ground surface elevation in Global Mapper within the assessment area (outlined in red) for Mar 2011 (T+T, 2015).

Table 4. Raw liquefaction-induced ground surface subsidence using original LiDAR points.

Earthquake Event(s)	Average Ground Surface Subsidence (mm)		
	10-m Buffer	20-m Buffer	50-m Buffer
Sep 2010	134	138	124
Feb 2011	214	213	148
Jun 2011	114	98	75
Dec 2011	7	12	15
CES	469	461	362

Table 5. LiDAR flight error adjustments, global adjustments for the difference between average LiDAR point elevations and benchmark survey elevations, and vertical tectonic movement adjustments.

Earthquake Event(s)	Adjustments (mm)		
	LiDAR Flight Error	Global Offset	Tectonic Vertical Movement
Sep 2010	-100	-3	0
Feb 2011	100	16	-85
Jun 2011	0	38	-40
Dec 2011	0	-65	0
CES	0	-14	-125
Any LiDAR survey affected by ejecta?			No

Note: The negative sign indicates the subtraction from the ground surface subsidence, while the positive sign indicates the addition to the ground surface subsidence.

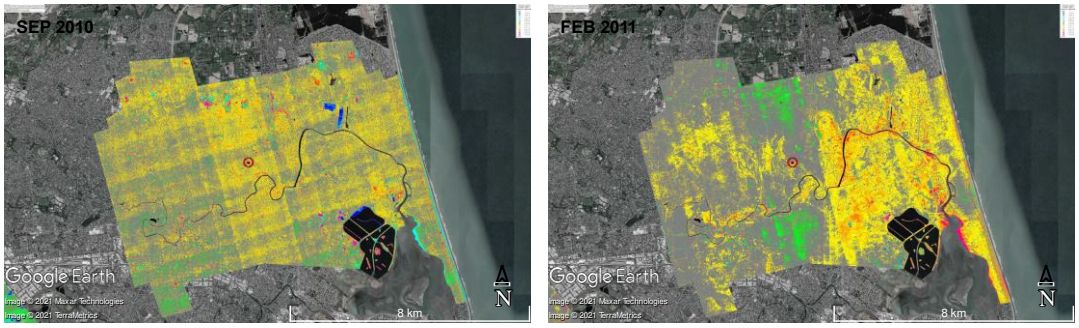


Figure 8. Vertical Ground Movements (adjusted for the tectonic component) for the Sep 2010 and Feb 2011 earthquakes (CGD, 2012b) – the site is in the zone of overestimated ground surface subsidence for the Sep 2010 earthquake and the zone of underestimated ground surface subsidence for the Feb 2011 earthquake.

Table 6. Corrected liquefaction-induced ground subsidence using Table 4 values and Table 5 adjustments.

Earthquake Event(s)	Average Calculated Ground Surface Subsidence (mm)		
	10-m Buffer	20-m Buffer	50-m Buffer
Sep 2010	31±75	35±75	21±75
Feb 2011	245±25	244±25	179±25
Jun 2011	112±25	96±25	73±25
Dec 2011	-58±50	-53±50	-50±50
CES	330±75	322±75	223±75

Notes: Positive values indicate ground surface subsidence; negative values indicate ground surface uplift.

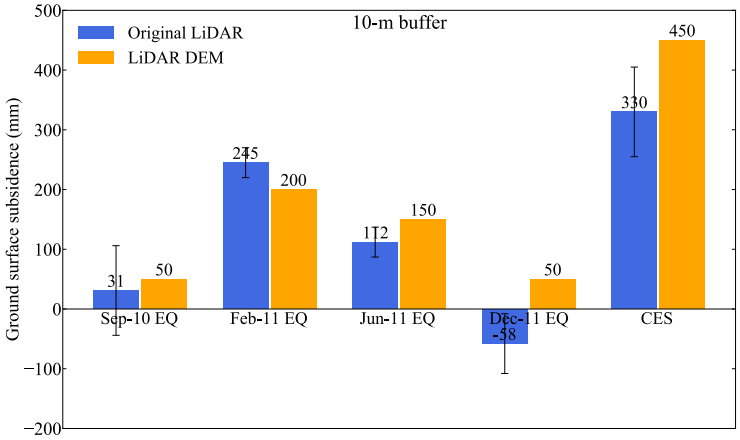


Figure 9. Comparison between the ground surface subsidence determined using the individual LiDAR elevation points and the ground surface subsidence estimated using the LiDAR DEMs.

Table 7. Ejecta-induced settlement for the top 20 m of the soil profile within the 10-m buffer for the 50th %ile PGA, P_L=50%, and C_{FC}=0.13 using BI-2016, ZRB-2002, and I_C cutoff of 2.6.

Earthquake Event	M_W	PGA (g)	Depth to Groundwater (m)	S_T (mm)	S_{V1D} (mm)	$S_{E,L}$ (mm)
Sep 2010	7.1	0.19	2.5	31±75	7±20	24±78
Feb 2011	6.2	0.38	2.5	245±25	71±50	174±56
Jun 2011	6.2	0.22	2.2	112±25	10±25	102±35
Dec 2011	6.1	0.26	2.0	-58±50	25±50	-83±71

Notes: S_T = Total liquefaction-induced settlement (Table 6); S_{V1D} = Average vertical settlement due to volumetric compression using the Boulanger and Idriss (2016) (BI-2016) and Zhang et al. (2002) (ZRB-2002) procedures and the de Greef and Lengkeek (2018) thin-layer correction procedure; $S_{E,L}$ = Ejecta-induced settlement as the difference between the LiDAR-based S_T and S_{V1D}.

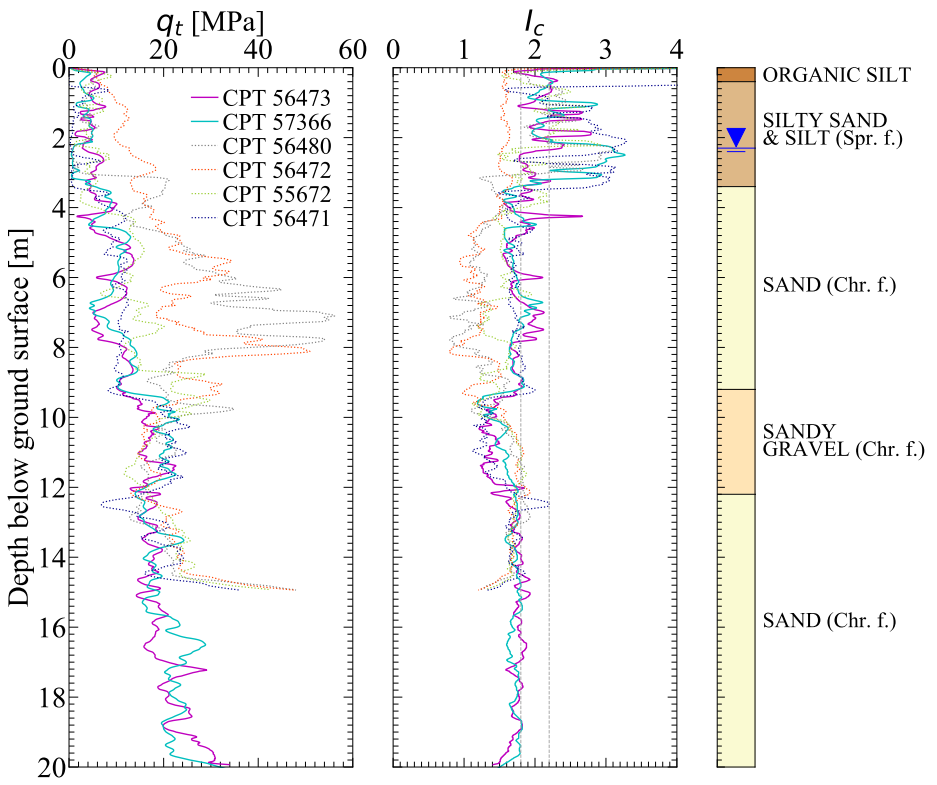


Figure 10. CPT traces and simplified soil profile for Shirley Intermediate School. (The soil layer colors are arbitrary.)

Table 8. CPT-based results for Shirley Intermediate School.

Earthquake Event	Parameter	CPT ID					
		56473	57366	56480	56472	55672	56471
Sep 2010	S_{V1D} (mm)	7	7	1	0	4	1
	LSN	1	1	0	0	1	0
	LPI	0	0	0	0	0	0
	LPI_{ish}	0	0	0	0	0	0
	$D_{FS<1}$ (m)	undet.	undet.	undet.	undet.	undet.	undet.
Feb 2011	S_{V1D} (mm)	71	70	7	0	43	36
	LSN	13	13	2	0	11	7
	LPI	5	5	1	0	4	1
	LPI_{ish}	3	4	1	0	3	1
	$D_{FS<1}$ (m)	3.20	3.18	undet.	undet.	2.72	3.45
Jun 2011	S_{V1D} (mm)	9	10	1	0	7	1
	LSN	2	2	1	0	2	0
	LPI	0	0	0	0	0	0
	LPI_{ish}	0	0	0	0	0	0
	$D_{FS<1}$ (m)	undet.	undet.	undet.	undet.	undet.	undet.
Dec 2011	S_{V1D} (mm)	22	28	4	0	20	6
	LSN	4	6	1	0	6	1
	LPI	0	1	0	0	1	0
	LPI_{ish}	0	1	0	0	1	0
	$D_{FS<1}$ (m)	4.27	4.32	undet.	undet.	3.45	undet.

Notes: $D_{FS<1}$ = Depth to the first liquefiable layer (FS_L<1) that is at least 200 mm thick, as determined by the Boulanger and Idriss (2016) liquefaction-triggering procedure (P_L=50%, C_{FC}=0.13, and $I_{c,cutoff}$ =2.6), and exported from Cliq v.3.0.3.2; undet. = the specified soil layer was not detected; LPI_{ish} = Ishihara-inspired LPI by Maurer et al. (2015).

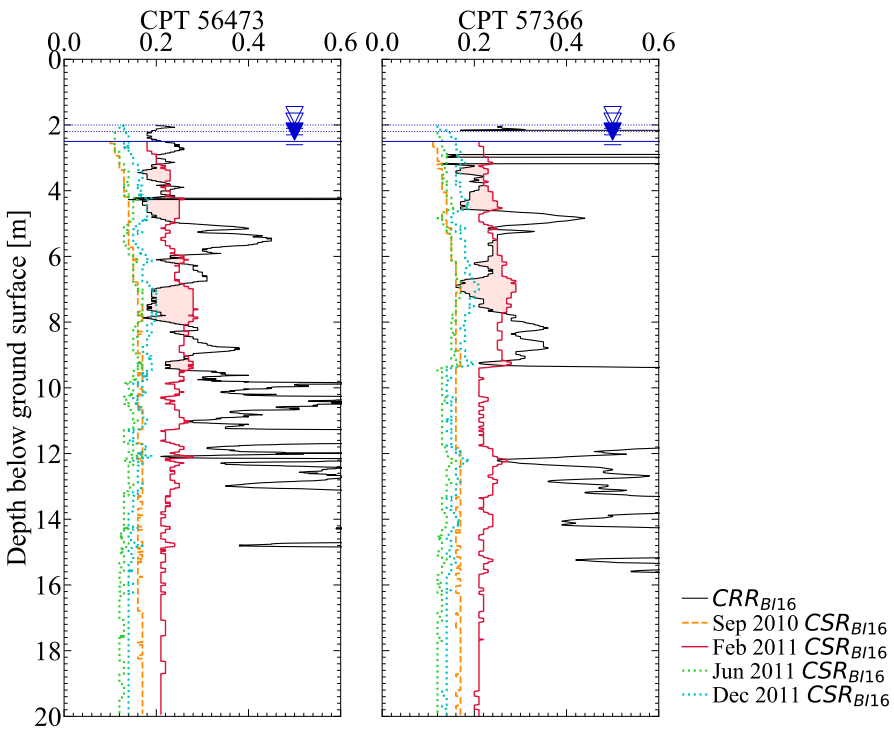


Figure 11. The Boulanger and Idriss (2016) estimated cyclic resistance (CRR_{BI16}) and the cyclic stress ratio (CSR_{BI16}) adjusted for M_w = 7.5 and σ'_{vo} = 1 atm for the Sep 2010, Feb 2011, Jun 2011, and Dec 2011 earthquakes for CPTs 56473 and 57366 at Shirley Intermediate School. Layers with FS_L < 1 for the Feb 2011 event are shaded.

The $S_{E,L}$ values in Table 7 were used in combination with the areal $S_{E,P}$ values in Table 3 to provide the best final estimate of ejecta-induced free-field settlement, $S_{E,final}$ (Table 9). The mean and the estimated uncertainty for $S_{E,final}$ are rounded to the nearest 5 mm to indicate an inclusive range of possible $S_{E,final}$ values for comparison among the sites in this study. Due to the inherent uncertainty in estimating ejecta-induced settlement, these values should be rounded off to the nearest 10 mm for practical engineering purposes. The $S_{E,final}$ represents the weighted average of $S_{E,L}$ and $S_{E,P}$ with respective weight coefficients of 1/3 and 2/3 for the Feb 2011 and Jun 2011 earthquakes and the respective weight coefficients of 0 and 1 for the Sep 2010 and Dec 2011 earthquakes. The lower weight coefficient for the Feb 2011 and Jun 2011 earthquakes was assigned to $S_{E,L}$ because the Shirley Intermediate School site was in the zone of overestimated/underestimated ground surface movements for the Sep 2010/Feb 2011 earthquake due to the LiDAR flight error and had slight to moderate underestimation of liquefaction manifestation at the ground surface (Maurer et al. 2014). $S_{E,L}$ was assigned 0 weight for the Sep 2010 and Dec 2011 earthquakes due to the absence of ejecta for the Sep 2010 earthquake and due to negligible ejecta and negative $S_{E,L}$ values for the Dec 2011 earthquake. The best estimates of the ejecta-induced free-field ground settlement at the Shirley Intermediate School site for the Sep 2010, Feb 2011, Jun 2011, and Dec 2011 earthquakes are 0 mm, 125 ± 25 mm, 50 ± 15 mm, and <5 mm, respectively, considering that the 10-m buffer is the most representative buffer in terms of spatial distribution of ejecta across the site.

Table 9. Best estimates of areal ejecta-induced settlement for Shirley Intermediate School.

Earthquake Event	10-m Buffer			20-m Buffer			50-m Buffer		
	$S_{E,L}$ (mm)	$S_{E,P}$ (mm)	$S_{E,final}$ (mm)	$S_{E,L}$ (mm)	$S_{E,P}$ (mm)	$S_{E,final}$ (mm)	$S_{E,L}$ (mm)	$S_{E,P}$ (mm)	$S_{E,final}$ (mm)
Sep 2010	24±78	0	0	28±78	0	0	18±78	0	0
Feb 2011	174±56	101±25	125±25	173±56	131±34	145±30	141±56	76±19	100±25
Jun 2011	102±35	23±12	50±15	86±35	31±16	50±15	68±35	20±10	35±15
Dec 2011	-83±71	≈0	<5	-78±71	≈0	<5	-63±71	≈0	<5

Notes: $S_{E,L}$ = Ejecta-induced settlement based on LiDAR data and reported in Table 7; $S_{E,P}$ = Median ejecta-induced settlement for the range of values in Table 3; $S_{E,final}$ = Best final estimate of ejecta-induced settlement rounded to the nearest 5 mm; Final plus/minus values are also rounded to the nearest 5 mm.

The soil profile at the Shirley Intermediate School site indicates a thick, clean sand site. A borehole log at the center of the site and the CPTs indicate a 5.5 m thick layer of fine to medium sand, SP, in the upper 10 m (from the 3.5 m to 9 m depth) and below the average groundwater depth of approximately 2.3 m BGS (Figure 10). This marine/estuarine SP layer of the Christchurch formation has an average q_t of 9 MPa. The top 3.5 m of the soil profile consist of the 0.4 m thick organic silty, OL, topsoil ($q_{t,avg}$ = 4 MPa) and underlying interchangeable layers of alluvial non-plastic to low plasticity silt, ML, and alluvial silty sand, SM, of the Springston formation ($q_{t,avg}$ = 4 MPa). Below the 9 m depth, sandy subrounded marine/estuarine gravel, GW, with $q_{t,avg}$ = 18 MPa extends to a depth of 12 m and overlies fine to coarse marine/estuarine sand, SP, which extends to a depth of 20 m. The provided q_t values corrected for thin-layer effects using the de Greef and Lengkeek (2018) procedure are based on CPTs 56473 and 57366. Two additional CPTs from outside the 50-m buffer show the presence of gravelly layers at depths shallower than 8 m close to the rim of the 50-m buffer.

CPTs 56473 and 57366, as the CPTs within the most representative buffer at the Shirley Intermediate School site, i.e., the 10-m buffer, were used to estimate the average crust thickness. The depth to the first $FS_L < 1$ layer that is at least 200 mm thick was 3.2 m and 4.3 m for the Feb 2011 and Dec 2011 earthquakes, respectively. For the Sep 2010 and Jun 2011 earthquakes, the 200 mm thick layer with $FS_L < 1$ did not exist (Table 8). The average crust thickness was also defined as the depth to the first $I_c < 2.6$ layer that is at least 200 mm thick and below the groundwater level; these values are provided in the *EjectaCaseHistories_FlatFile.xlsx* spreadsheet. They were estimated as 2.8 m, 2.8 m, 2.7 m, and 2.6 m BGS for the Sep 2010, Feb 2011, Jun 2011, and Dec 2011 earthquakes, respectively. For the most representative buffer, i.e., the 10-m buffer, the average LPI = 0, 5, 0, and 1 and LSN = 1, 13, 2, and 5 for the Sep 2010, Feb 2011, Jun 2011, and Dec 2011 earthquakes, respectively, based on CPTs 56473 and 57366. Considering the percent coverage of the unobstructed area of the 10-m buffer by liquefaction ejecta (Figure 6), the severity of liquefaction manifestation at the ground surface was none (i.e., 0 %), extreme (i.e., 50%-100%), severe (i.e., 20%-50%), and minor (i.e., < 5 %) for the Sep 2010, Feb 2011, Jun 2011, and Dec 2011 earthquakes, respectively. Thus, the severity of surficial manifestation of liquefaction was significantly higher than estimated by LPI or LSN for the Feb 2011 and Jun 2011 earthquakes, slightly underestimated for the Dec 2011 earthquake, and correctly estimated for the Sep 2010 earthquake. Similarly, the average L_D of 0, 77, 1, and 8 kN/m and C_R of 46, 46, 44, and 43 kN/m for the Sep 2010, Feb 2011, Jun 2011, and Dec 2011 earthquakes, respectively, capture well the severity of liquefaction manifestation at the site for the Sep 2010 earthquake, underestimate it slightly for the Feb 2011 earthquake, underestimate it significantly for the Jun 2011 earthquake, and overestimate it slightly for the Dec 2011 earthquake, according to the L_D-C_R chart developed by Hutabarat and Bray (2022).

CONCLUSION

The liquefaction ejecta-induced free-field settlement at 61 sites in Christchurch was estimated for each of the four major Canterbury earthquakes using photographic evidence and airborne LiDAR survey elevation points because direct measurements of ejected soil and the associated settlement were not available. The best estimate of ejecta-induced settlement was calculated as the weighted average of the two estimates. The *EjectaCaseHistories_FlatFile.xlsx* spreadsheet summarizes key characteristics of the 61 sites and the ejecta-induced settlement at each of these sites for each of the four main earthquakes. The flat file also lists the sites from the "55 sites" dataset that were not considered for the ejecta-induced settlement analysis (e.g., due to lateral spreading) as well as the sites for which the best final estimates of ejecta-induced settlement were provided without detailed analyses.

The photographic evidence-based approach for estimating the ejecta-induced settlement relies on high-resolution aerial photographs, ground photographs, and the detailed inspection notes for individual properties by the EQC LDAT comprised of engineers, engineering geologists, and engineering technicians. The area of a site covered with ejecta was measured approximately by utilizing the Google Earth Pro tools on the high-resolution aerial photograph supplied for each earthquake event. The height of ejecta was estimated based on ground photographs and detailed LDAT property inspection notes that had measurements of ejecta remnants. The uncertainty in estimating the height of ejecta was accounted for by providing a range of potential heights rather than a single value.

The LiDAR-based approach for estimating the ejecta-induced settlement made use of elevation points surveyed by airborne LiDAR prior to and after each major earthquake event. The pre-earthquake and post-earthquake ground surface elevations were averaged in Global Mapper over the assessment area of a site and the difference between the two elevations was the earthquake-induced ground surface subsidence. The earthquake-induced ground surface subsidence was then adjusted for the vertical tectonic movement, artifacts of LiDAR (flight error bands), and global offset due to the median approximate error of each pre- and post-earthquake LiDAR survey relative to the GPS-surveyed benchmark points to obtain the liquefaction-induced ground settlement. The accuracy of the surveyed LiDAR elevation points was ±70 mm for all surveys except for the

Jul 2003 survey that had the vertical accuracy of ±150 mm. The errors related to LiDAR measurements supported the range of liquefaction-induced settlement estimates. The ejecta-induced settlement was obtained by subtracting the volumetric-induced settlement, which was calculated using the Zhang et al. (2002) procedure.

The best estimate of ejecta-induced settlement was calculated by assigning weights to each of the two estimated values described previously. This was done on a site-by-site basis, and it depended on site conditions, including the site's location relative to the LiDAR flight error bands, liquefaction performance of soil at the site relative to the estimations made by liquefaction triggering procedures, and reasonableness of values estimated by the LiDAR. There were cases of negligible ejecta observed at the site as evidenced by the photographs, yet LiDAR-based values indicated significant ejecta-induced settlement. Additionally, the LiDAR approach in a few cases estimated ground uplift (i.e., negative ejecta-induced settlement), although accounting for the uncertainty of the estimate typically led to a reasonable settlement value being within a range of values estimated using photographic evidence.

The aerial LiDAR was found to be a good means of estimating ground surface subsidence on a regional scale. However, errors associated with the LiDAR flights can become significant for individual sites that typically have the ground surface subsidence within the LiDAR margin of error. The LiDAR measurements are also affected by vegetation and topographic features such as undulations that appeared at many sites in Christchurch following the earthquakes. The uncertainty in the LiDAR-based approach can also be attributed to the vertical tectonic movements that resulted from each earthquake. Subtracting the volumetric-induced settlement from the LiDAR-based liquefaction-induced settlement further added to the uncertainty associated with the estimates of ejecta-induced settlement.

The photographic evidence generally provided more consistent results of ejecta-induced settlement, mainly due to the method's dependence on the area covered by ejecta, which could be obtained with reasonable confidence. Geometrically approximating the complex shapes of ejecta introduced some uncertainty; however, the greatest uncertainty in the method could be ascribed to estimating the height of ejecta, especially in the absence of ground photographs and detailed property inspection notes. Additionally, grass could obscure ejecta.

Nevertheless, the analyzed geotechnical database for the 2010-2011 Canterbury earthquakes provides a good set of data for developing detailed ejecta case histories. Rarely is there the wealth of data related to liquefaction-induced land damage as those for the 2010-2011 CES, since few countries in earthquake-prone regions have residential land insured for damage from natural disasters. Also, rarely does a single site experience significant, repeated liquefaction and formation of ejecta under varying levels of ground motion in a short span of time, like the sites in Christchurch. Therefore, the detailed 235 case histories developed in this study constitute a unique database that can be used to examine the occurrence and effects of ejecta. The data provide a reasonable basis for the development of a procedure to evaluate when liquefaction ejecta will or will not occur and to estimate the quantity of ejecta in earthquakes.

Post-earthquake reconnaissance teams should take direct measurements of ejecta immediately after future earthquakes while all related evidence remains intact. This can be performed by utilizing terrestrial LiDAR, structure-from-motion photogrammetry, or conventional land surveys, photographs, and hand measurements. The volume of ejecta can also be measured by placing the ejected soil into standard-size buckets. For regional assessment of liquefaction-induced damage, strict control of ground points is recommended. The inspection teams can use individual property maps to add locations of ejecta and sketch their approximate shapes. Many high-quality ground photographs with measurement placards should be taken. Subsurface investigations such as CPT soundings, soil sampling, groundwater measurements, and shear wave and compressional wave velocity measurements can be performed later at sites. With reliable PGA estimates, this information would provide an excellent set of data that can be interrogated and appended to the database developed in this study with an aim of developing a robust procedure for estimating the ejecta-induced settlement.

ACKNOWLEDGMENTS

This research was supported primarily by the U. S. Geological Survey (USGS), Department of Interior, under USGS award number G20AP00079. Additional support was provided by the U.S. National Science Foundation through Grant CMMI-1956248 and by the Faculty Chair in Earthquake Engineering Excellence at UC Berkeley. The views and conclusions contained in this document are those of the authors and should not be interpreted as necessarily representing the official policies, either expressed or implied, of the U.S. Government. The authors would like to extend their gratitude to James Russell, Oliver Hay, and Nathan McDougall of Tonkin and Taylor, Ltd., New Zealand, for their help on this project. The

authors would also like to thank Prof. Misko Cubrinovski of the Univ. of Canterbury for valuable comments and Dr. Daniel Hutabarat of UC Berkeley for providing the code to compute the liquefaction ejecta demand and crust resistance parameters.

ELECTRONIC SUPPLEMENTS

All details of the four case histories for each of the 61 sites are provided as an electronic supplement to this paper as Appendix A.1 through Appendix A.61. The important information for each of the case histories for each site is provided in the *EjectaCaseHistories_FlatFile.xlsx* spreadsheet as an electronic supplement to this paper. Raw CPT data are publicly available through the New Zealand Geotechnical Database (NZGD).

REFERENCES

Beyzaei, C. Z., Bray, J. D., van Ballegooy, S., Cubrinovski, M., and Bastin, S. (2018). "Depositional environment effects on observed liquefaction performance in silt swamps during the Canterbury earthquake sequence." *Soil Dynamics and Earthquake Engineering*, 107, 303-321.

Boulanger, R. W., and Idriss, I. M. (2016). "CPT-based liquefaction triggering procedure." *J. of Geotechnical and Geoenvironmental Engineering*, 142(2), 1-11.

Bradley, B. A., and Hughes, M. (2012a). *Conditional Peak Ground Accelerations in the Canterbury Earthquakes for Conventional Liquefaction Assessment* Technical Report prepared for the Department of Building and Housing, New Zealand.

Bradley, B. A., and Hughes, M. (2012b). *Conditional Peak Ground Accelerations in the Canterbury Earthquakes for Conventional Liquefaction Assessment: Part 2*, Technical Report prepared for the Ministry of Business, Innovation and Employment, New Zealand.

Bray, J. D., and Dashti, S. (2014). "Liquefaction-induced building movements." *Bulletin of Earthquake Engineering*, 12, 1129–56.

Bray, J.D. and Macedo, J. (2017). "6th Ishihara Lecture: Simplified procedure for estimating liquefaction-induced building settlement." *Soil Dynamics and Earthquake Engineering J.*, 102, 215-231.

Canterbury Earthquake Recovery Authority (CERA). (2014). "Verification of LiDAR acquired before and after the Canterbury Earthquake Sequence," *Technical Specification*, <https://canterburygeotechnicaldatabase.projectorbit.com> (May, 2022)

Canterbury Geotechnical Database (2012a) "Aerial Photography", *Map Layer CGD0100 - 1 Jun 2012*, retrieved Jul 2018 – Jul 2021 from <https://canterburygeotechnicaldatabase.projectorbit.com/> (Jul., 2018 – Jul., 2021).

Canterbury Geotechnical Database (2012b) "Vertical Ground Surface Movements", *Map Layer CGD0600 - 23 Jul 2012*, <https://canterburygeotechnicaldatabase.projectorbit.com/> (Jul., 2018 – Jul., 2021).

Canterbury Geotechnical Database (2014) "Event Specific Groundwater Surface Elevations", *Map Layer CGD0800 - 10 Jun 2014*, from <https://canterburygeotechnicaldatabase.projectorbit.com/> (Jul., 2018 – Jul., 2021).

Canterbury Geotechnical Database (2015) "Conditional PGA for Liquefaction Assessment", *Map Layer CGD5110 - 20 Jul 2015*, <https://canterburygeotechnicaldatabase.projectorbit.com/> (Jul., 2018 – Jul., 2021).

Cubrinovski, M., Rhodes, A., Ntritsos, N., and van Ballegooy, S. (2017). "System response of liquefiable deposits." In *Proceedings of the 3rd International Conference on Performance-based Design in Earthquake Geotechnical Engineering*, Vancouver, BC.

de Greef, J., and Lengkeek, H. J. (2018). "Transition and thin layer corrections for CPT based liquefaction analysis." *Proceedings of the 4th International Symposium on Cone Penetration Testing (CPT'18)*, Delft, The Netherlands.

GNS Science. (2021). "The most recent aftershock map." <https://www.gns.cri.nz/Home/Our-Science/Natural-Hazards-and-Risks/Recent-Events/Canterbury-quake/Recent-aftershock-map> (Aug. 1, 2021)

Hutabarat, D., and Bray J. D. (2022). "Estimating the severity of liquefaction ejecta using the cone penetration test." *J. of Geotechnical and Geoenvironmental Engineering*, ASCE, 148(3), 04021195.

Ioannides, J. T. (2019). "Cliq v.3.0.3.2 – CPT soil liquefaction software." *Greece: Geologismiki*.

Iwasaki, T., Tatsuoka, F., Tokida, K., and Yasuda, S. (1978). "A practical method for assessing soil liquefaction potential based on case studies at various sites in Japan." *Proceedings of the 2nd International Conference on Microzonation*, 885-896, National Science Foundation, Washington, DC.

Land Damage Assessment Team (LDAT). (2021). "LDAT Reports Data Entry" *(Database)*. <https://tracker.projectorbit.com/Sites/LDAT/EQCFieldReportFormExtra.aspx>.

Lees, J., van Ballegooy, S., and Wentz, F. J. (2015). "Liquefaction susceptibility and fines content correlations of Christchurch soils." *6th International Conference on Earthquake Geotechnical Engineering*, Christchurch, New Zealand.

Maurer, B. W., Green, R. A., Cubrinovski, M., and Bradley, B. A. (2014). "Evaluation of the liquefaction potential index for assessing liquefaction hazard in Christchurch, New Zealand." *J. of Geotechnical and Geoenvironmental Engineering*, 140(7), 04014032-1-11.

Maurer, B. W., Green, R. A., Cubrinovski, M., and Bradley, B. (2015). "Assessment of CPT-based methods for liquefaction evaluation in a liquefaction potential index framework." *Géotechnique*, 65(5), 328–336.

Maurer, B., Green, R., van Ballegooy, S., and Wotherspoon, L. (2019). "Development of region-specific soil behavior type index correlations for evaluating liquefaction hazard in Christchurch, New Zealand." *Soil Dynamics and Earthquake Engineering*, 117, 96-105.

Obermeier, S. F. (1996). "Use of liquefaction-induced features for paleoseismic analysis." *Engineering Geology*, 44, 1-76.

Rogers, N., van Ballegooy, S., Williams, K., and Johnson, L. (2015). "Considering post-disaster damage to residential building construction - Is our modern building construction resilient?" *6th International Conference on Earthquake Geotechnical Engineering*, Christchurch, New Zealand.

Russell, J., and van Ballegooy, S. (2015). *Canterbury Earthquake Sequence: Increased Liquefaction Vulnerability Assessment Methodology*, T+T Report 0028-1-R-JICR-2015 prepared for the Earthquake Commission.

Tonkin and Taylor, Ltd. (T+T). (2013). *Liquefaction Vulnerability Study - Report to Earthquake Commission*, Report T&T.

Tonkin and Taylor, Ltd. (T+T). (2015). "Tonkin and Taylor Geotechnical Database: Canterbury Maps", *(Database)*. <https://canterburygeotechnicaldatabase.projectorbit.com/>.

van Ballegooy, S., S., Malan, P., Lacrosse, V., Jacka, M., Cubrinovski, M., Bray, J. D., O'Rourke, T. D., Crawford, S. A., and Cowan, H. (2014). "Assessment of liquefaction-induced land damage for residential Christchurch." *Earthquake Spectra*, 30(1), 31-55.

Zhang, G., Robertson, P. K., and Brachman, R. W. I. (2002). "Estimating liquefaction-induced ground settlements from CPT for level ground." *Can. Geotech. J.*, 39, 1168-1180.

The open access Mission of the International Journal of Geoengineering Case Histories is made possible by the support of the following organizations:



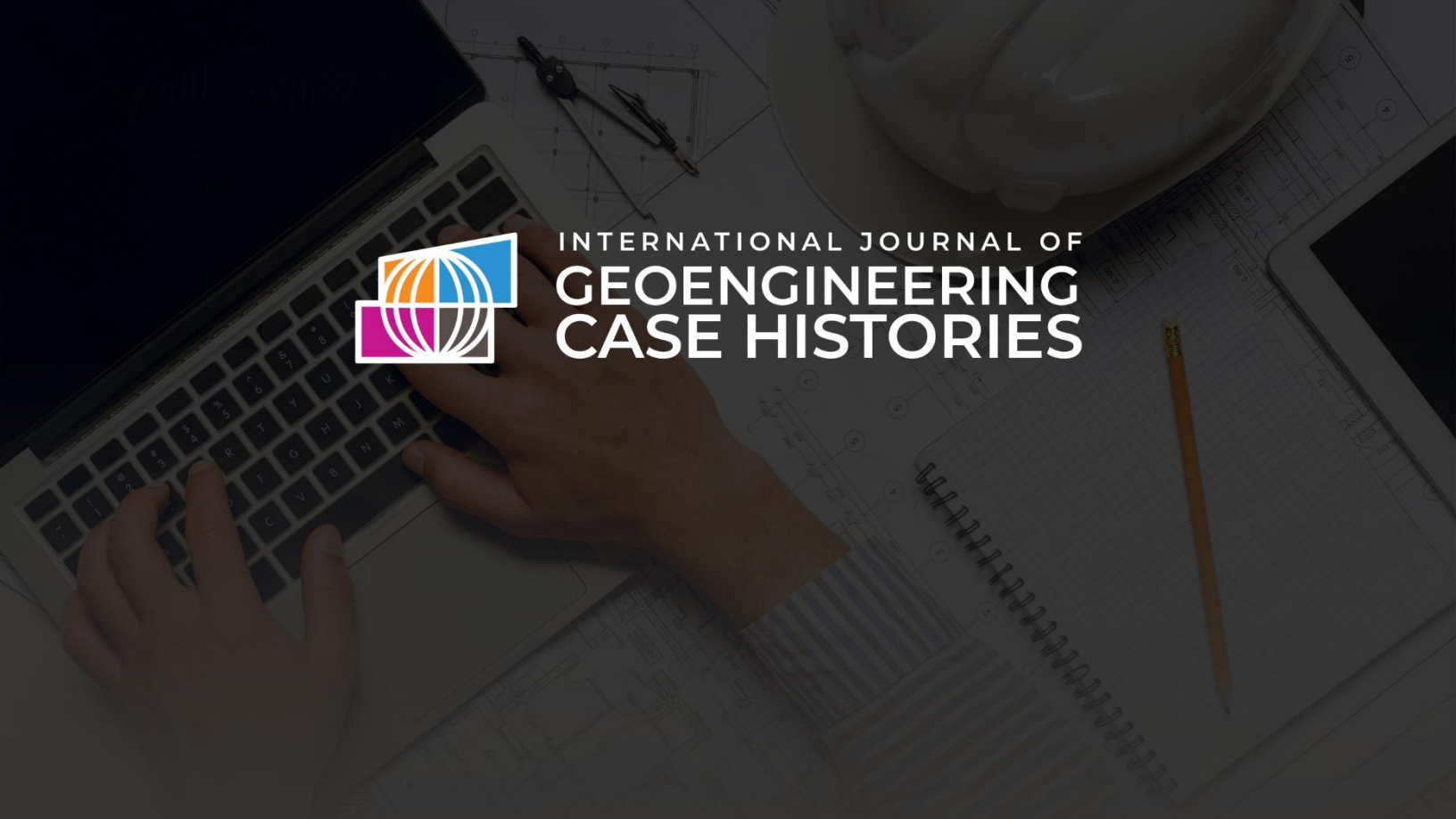








Access the content of the ISSMGE International Journal of Geoengineering Case Histories at:
https://www.geocasehistoriesjournal.org



INTERNATIONAL JOURNAL OF
GEOENGINEERING
CASE HISTORIES

The Journal's Open Access Mission is generously supported by the following Organizations:

dar
a Sidara company

Geosyntec consultants
engineers | scientists | innovators

ConeTec
MUD BAY DRILLING
LANKELMA
Geotech DRILLING

ENGEO
Expect Excellence

Access the content of the ĪSSMGE Īnternational Journal of Geoengineering Case Histories at:
www.geocasehistoriesjournal.org

Downloaded: Thursday, November 19 2026, 08:40:42 UTC